



## Coulomb oscillations based on band-to-band tunneling in a degenerately doped silicon metal-oxide-semiconductor field-effect transistor

Kyung Rok Kim, Dae Hwan Kim, Jong Duk Lee, and Byung-Gook Park

Citation: *Applied Physics Letters* **84**, 3178 (2004); doi: 10.1063/1.1707217

View online: <http://dx.doi.org/10.1063/1.1707217>

View Table of Contents: <http://scitation.aip.org/content/aip/journal/apl/84/16?ver=pdfcov>

Published by the [AIP Publishing](#)

---

### Articles you may be interested in

[Single hole transport in a silicon metal-oxide-semiconductor quantum dot](#)

*Appl. Phys. Lett.* **103**, 163508 (2013); 10.1063/1.4826183

[Experimental study on quantum confinement effects in silicon nanowire metal-oxide-semiconductor field-effect transistors and single-electron transistors](#)

*J. Appl. Phys.* **103**, 053709 (2008); 10.1063/1.2874247

[Valence band structure of ultrathin silicon and germanium channels in metal-oxide-semiconductor field-effect transistors](#)

*J. Appl. Phys.* **98**, 024504 (2005); 10.1063/1.1948528

[Coulomb blockade oscillations in ultrathin gate oxide silicon single-electron transistors](#)

*J. Appl. Phys.* **97**, 116106 (2005); 10.1063/1.1921335

[Extension of Coulomb blockade region by quantum confinement in the ultrasmall silicon dot in a single-hole transistor at room temperature](#)

*Appl. Phys. Lett.* **84**, 3172 (2004); 10.1063/1.1710709

---

A horizontal banner with an orange-to-yellow gradient background. The text '2014 Special Topics' is centered in a large, white, sans-serif font. Below the text are five circular icons, each containing a different material structure and a label: 'PEROVSKITES' (red and black lattice), '2D MATERIALS' (blue and red lattice), 'MESOPOROUS MATERIALS' (green and blue porous structure), 'BIOMATERIALS/ BIOELECTRONICS' (yellow and black structure), and 'METAL-ORGANIC FRAMEWORK MATERIALS' (brown and black structure). At the bottom left is the 'AIP | APL Materials' logo, and at the bottom right is a red ribbon with the text 'Submit Today!' in white.

2014 Special Topics

PEROVSKITES

2D MATERIALS

MESOPOROUS MATERIALS

BIOMATERIALS/ BIOELECTRONICS

METAL-ORGANIC FRAMEWORK MATERIALS

AIP | APL Materials

Submit Today!

# Coulomb oscillations based on band-to-band tunneling in a degenerately doped silicon metal-oxide-semiconductor field-effect transistor

Kyung Rok Kim,<sup>a)</sup> Dae Hwan Kim, Jong Duk Lee, and Byung-Gook Park  
*Inter-University Semiconductor Research Center (ISRC), and School of Electrical Engineering,  
 Seoul National University, San 56-1, Shinlim-dong, Kwanak-gu, Seoul 151-742, Korea*

(Received 12 November 2003; accepted 20 February 2004)

We report Coulomb oscillations based on band-to-band tunneling through a valence band in silicon metal-oxide-semiconductor field-effect transistors. Degenerately  $p^+$ -doped channel and  $n^+$ -doped source/drain enables band-to-band tunneling, which can play a major role in the transport between the channel and source/drain. The formation of tunnel barriers and a quantum dot in a single-electron transistor structure originates from two  $p^+ - n^+$  tunnel junctions and a  $p^+$ -doped channel with mesoscopic dimension, respectively. Coulomb-blockade oscillations with multiple peaks were clearly observed at liquid nitrogen temperature. Using the electrical and thermal characterization of the quantum dot, single-electron charging effect based on band-to-band tunneling is confirmed. © 2004 American Institute of Physics. [DOI: 10.1063/1.1707217]

Since Coulomb blockade of single-electron tunneling was proposed with a theoretical prediction<sup>1,2</sup> and demonstrated in a metallic system,<sup>3</sup> there have been extensive investigations on single-electron charging effects in semiconductor nanostructures in which quantum-mechanical effects are strongly manifested. After the pioneering work of Scott-Thomas *et al.*,<sup>4</sup> single-electron tunneling phenomena in semiconductors through an impurity potential, such as localized electron states or trapped charge,<sup>5,6</sup> were reported in moderately doped silicon (Si) quantum wires or metal-oxide-semiconductor field-effect transistor (MOSFET) structures, which have ample room for forming ultrasmall island and barriers by conventional process technology. As the miniaturization of device dimension continues, single-electron tunneling becomes a prominent and ubiquitous phenomenon. On the one hand, in pursuit of single-electron transistors (SETs) with practical functionality, various SETs with on the basis of Si MOSFET structure were implemented with definite formation mechanisms of intentional tunnel barriers and quantum dots (QDs), such as point-contact geometries,<sup>7</sup> depleting electrostatically a semiconductor depletion barriers under dual gates,<sup>8</sup> undulated gate oxide or silicon film,<sup>9</sup> and pattern deformation and band-profile modification due to oxide-induced stress.<sup>10</sup> These mechanisms were based on undoped Si in order to prevent the unintentional characteristics due to impurity potentials; thus, electron transport through a QD occurs only along in the conduction band. Single-electron tunneling based on band-to-band transport has been theoretically proposed,<sup>11</sup> and some experiments were performed in carbon nanotube systems,<sup>12,13</sup> but have not been observed or implemented in Si-based systems yet.

This letter reports the Coulomb-blockade oscillations based on band-to-band single-electron tunneling in a degenerately doped Si MOSFET without lightly doped source drain extensions. The fabricated device has a highly reproducible self-aligned structure, which provides a major advantage in miniaturization. The experimental characteristics with

total capacitance of 2 aF is demonstrated at 77 K, and the basis of the tunneling mechanism through the valence band is discussed.

The devices were fabricated on the  $4 \times 10^{15} \text{ cm}^{-3}$   $p$ -doped 40-nm-thick top layer of a silicon-on-insulator (SOI) wafer prepared by separation by implanted oxygen. This top layer is separated from the Si substrate by a 375-nm-thick buried oxide. Figure 1(a) shows a schematic of the fabricated device on an SOI substrate. SOI channel wires are formed by the *sidewall spacer patterning* method, which effectively suppressed the unintentional potential fluctuation along the narrow channel due to excellent uniformity.<sup>8,14-16</sup> After the SOI wire was defined, the remaining oxide was removed by wet etching and a 5-nm screen oxide was thermally grown at 800 °C.  $\text{BF}_2^+$  ions were implanted as channel

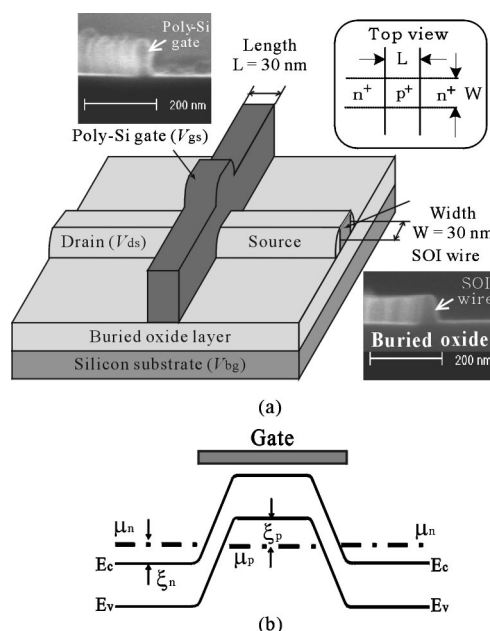


FIG. 1. (a) Schematic of the fabricated device for a degenerately doped sample. Cross-sectional SEM images of the 30-nm-wide SOI channel wire and poly-Si gate. The inset shows top view representing channel length  $L$  and width  $W$ . (b) Schematic energy band diagram of a degenerately doped sample along the channel surface under a gate at thermal equilibrium state.

<sup>a)</sup> Author to whom correspondence should be addressed; electronic mail: rocky@smdl.snu.ac.kr

dopants at 25 keV with doses of  $5 \times 10^{14} \text{ cm}^{-2}$  (degenerately doped sample) and  $5 \times 10^{13} \text{ cm}^{-2}$  (normally doped sample). During the formation of an oxide spacer around the SOI channel wire to reduce gate-to-dot capacitance ( $C_g$ ), the screen oxide was removed by dry etching in  $\text{CHF}_3/\text{CF}_4$  reactive-ion plasma, and 10-nm-thick thermal oxide was grown at  $800^\circ\text{C}$  for the gate dielectrics. Subsequently, an 80-nm-thick phosphorus-doped polycrystalline silicon (poly-Si) layer was deposited and patterned by the sidewall spacer patterning method to cross the SOI channel wire at right angles. Scanning electron microscopy (SEM) images in Fig. 1(a) show the 30-nm-wide SOI channel wire and poly-Si gate. As a result, the channel region is extremely shrunk down to mesoscopic dimensions, with 30-nm physical length and width. Contact areas were created by implanting the source and drain regions with dose of arsenic ions of  $5 \times 10^{15} \text{ cm}^{-2}$ , which is ten times larger than that of  $\text{BF}_2^+$  ions in the degenerately doped sample. In order to activate the dopants, the wafers were annealed at  $1000^\circ\text{C}$  for 10 s in a rapid thermal annealing system. Note that diffusion of arsenic ions under the gate reduces the effective channel length. After major thermal steps, boron concentration in the channel is about  $10^{20} \text{ cm}^{-3}$  for the degenerately doped samples. In case of the normally doped samples, we can estimate it to be about  $10^{18} \text{ cm}^{-3}$  level, which is smaller than the effective density of state ( $N_v$ ) in Si valence band. Consequently, the fabricated device has empty states in the valence band of  $p^+$ -doped channel region, which enable band-to-band tunneling. Figure 1(b) shows the energy band diagram of the fabricated device at a thermal equilibrium state. Degenerate doping concentration induces degeneracy in the channel ( $\xi_p$ :  $p$  side) and source/drain ( $\xi_n$ :  $n$  side); thus, the chemical potentials on the  $n$  side ( $\mu_n$ ) and  $p$  side ( $\mu_p$ ) are located within the allowed energy state on the conduction band  $E_c$  and valence band  $E_v$ , respectively. If the channel dimensions shrink down to the mesoscopic regime with this configuration of energy band, the extremely small channel acts as an island connected to the source and drain via  $p^+ - n^+$  tunnel junctions, through which tunneling occurs to conduct current, and the insulated poly-Si gate can control the surface channel (island) potentials.

The device was characterized by a precision semiconductor parameter analyzer (HP 4155A). Figure 2(a) shows the drain current  $I_{ds}$  measured at 77 K as a function of the gate voltage  $V_{gs}$  and the drain-source voltage  $V_{ds}$  for the degenerately doped sample. The clear rhombus-shaped valley caused by the Coulomb blockade is observed at liquid nitrogen temperature. From the slope of each side of the rhombus-shaped Coulomb blockade region, we can extract the ratio of the gate-dot ( $C_g$ ), drain-dot ( $C_d$ ), and source-dot ( $C_s$ ) capacitance as  $C_g:C_d:C_s=1:1.34:0.435$ . Therefore, the gain modulation factor  $\alpha$  is estimated to be 0.36. The single-electron addition energy  $E_a$  is well approximated by the sum of the Coulomb charging energy  $e^2/C_{\text{total}}$  and the quantized level separation  $\Delta E$  in the Si QD systems. Using  $\alpha$ , we can convert  $E_a$  to the gate voltage spacing between current peaks ( $\Delta V_g$ ):  $\Delta V_g = E_a/\alpha e$ . From Fig. 2(b),  $\Delta V_g$  is about 220 meV. The single-electron addition energy  $E_a$  is thus estimated to be 79.2 meV ( $\sim 10k_B T$ ). In addition, tunneling resistance of the tunnel junctions can be extracted

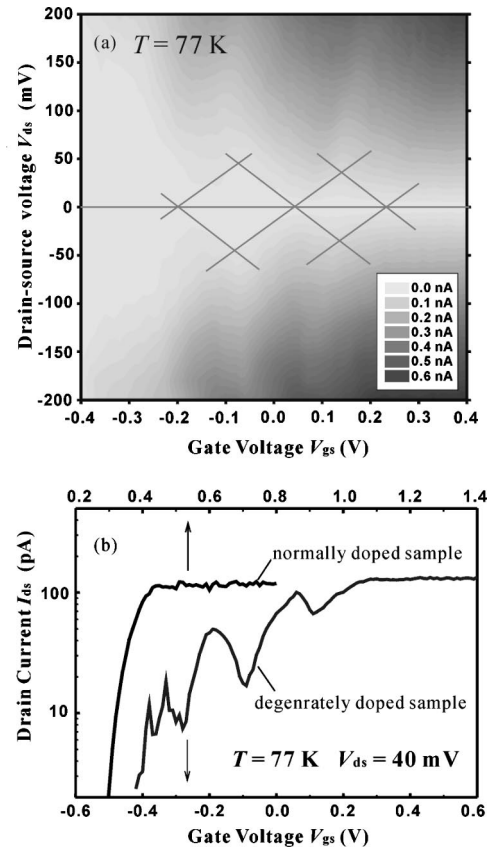


FIG. 2. (a) Contour plot of the drain-source current  $I_{ds}$  as a function of the  $V_{gs}$  and the  $V_{ds}$ , at 77 K. (b)  $I_{ds}-V_{gs}$  characteristics of fabricated devices normally doped ( $\sim 10^{18} \text{ cm}^{-3}$ ) and degenerately doped ( $\sim 10^{20} \text{ cm}^{-3}$ ) samples by the log-scale plot of the drain current  $I_{ds}$  at  $V_{ds}=40 \text{ mV}$ . The definite criterion of the doping concentration is the effective density of states in silicon valence band ( $N_v \sim 10^{19} \text{ cm}^{-3}$ ).

from the reciprocal of peak conductance in the measured characteristics [Fig. 2(b)], which is much higher than the resistance quantum ( $h/e^2 \sim 25.813 \text{ k}\Omega$ ). Thus, universal conductance fluctuations on the order of  $e^2/h^{17,18}$  are not appropriate to explain these oscillatory features. Therefore, this device is considered to satisfy the two main requirements for observing clear single-electron charging effects of typical single-electron devices.<sup>19</sup>

From the measured results, total capacitance of QD is evaluated as  $C_{\text{total}}=2.02 \text{ aF}$ . If we assume the island has a disk shape because the gate controls the surface potentials, the  $C_{\text{total}}$  corresponds to the self-capacitance of the disk with a diameter of 14.4 nm. Therefore, the effective size of the QD is estimated to be smaller than 14.4 nm, which is effectively shrunken by the reduced effective channel length and inherent depletion width of the tunnel junctions. The  $C_g$  of 0.73 aF corresponds to 40% of the gate capacitance obtained by the approximation of two parallel electrodes having the dielectrics of a 10-nm-thick oxide layer with a geometrically defined area. We also investigated the difference between normally doped and degenerately doped samples, as shown in Fig. 2(b). For a normally doped sample, typical  $n$ -channel MOSFET characteristics were observed at 77 K, while the degenerately doped sample shows a clear current oscillation in the subthreshold region. The origin of these oscillation peaks should be distinguished from work done on a similar



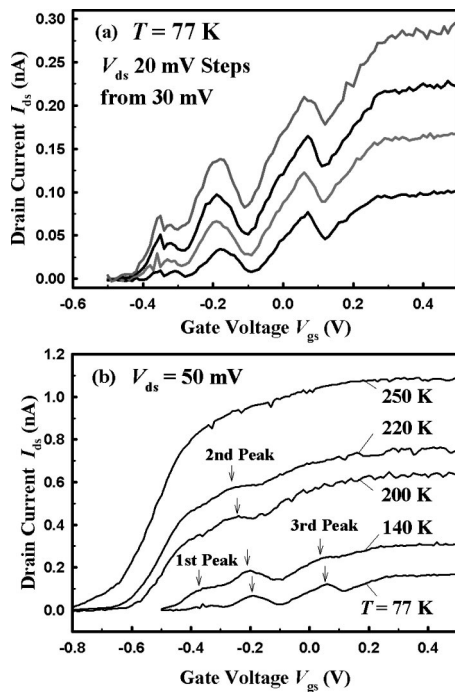


FIG. 3. (a)  $I_{ds}-V_{gs}$  characteristics as a function of  $V_{ds}$  for a degenerately doped sample at 77 K.  $V_{ds}$  is varied from 30 to 90 mV with 20 mV steps. (b)  $I_{ds}-V_{gs}$  characteristics as a function of the temperature at  $V_{ds}=50$  mV. The second peak with the highest band-to-band tunneling probability was observed, even at 220 K.

type of conventional bulk-Si or SOI MOSFET.<sup>6,20</sup> These studies attributed the conductance oscillation to Coulomb-blockade oscillation by randomly distributed channel impurity potential<sup>20</sup> or single disordered QD whose extension is comparable to the source-drain distance.<sup>6</sup> These results were characterized at or below liquid helium temperature and independent of the dopant concentration. However, our experiments show either clear or no oscillatory features dependent on the doping concentration with the definite criterion of the effective density of states. In addition, the extracted parameters are well matched to the geometrical dimensions of the device. These suggest that the observed single-electron phenomena can be attributed to the degenerately doped island with the Fermi level in the valence band between the two  $p^+-n^+$  tunnel junctions, not to the impurity potential.

Figure 3 shows the  $I_{ds}-V_{gs}$  curves as a function of  $V_{ds}$  and the environmental temperature. Three primary peaks and valleys, which maintain their number even at high  $V_{ds}$ , imply that the degenerate Si QD has three available energy states, whose number is limited by the upper limit of the valence band. In Fig. 3(b), as temperature increases from 77 to 250 K, the third current peak disappears first because of thermally activated current over the forbidden bandgap. The second peak, as the middle one of three primary current peaks, shows highest peak current when compared with the next valley current even at high temperature. This result is reasonable because the condition of second (middle) peak observation is maximum alignment between the electrons of source side and the available states in the valence band of the channel side, while the surface potential in the channel decreases by the gate voltage. Consequently, the enhanced band-to-band tunneling probability increases peak current.

Thus, these characteristics also confirm that single-electron charging effects originate from band-to-band tunneling via the valence band. In addition, the maximum temperature at which we can still observe the drain current oscillation is 220 K, which is superior to previously reported results in the Si MOSFETs without any additional electrodes or materials for tunnel barriers,<sup>6,20</sup> since our device has a definite mechanism of tunnel barriers and extremely small channel dimensions. If the patterning technology guarantees a sub-30 nm scale in the definition of channel region, the operation temperature can be increased to the room temperature. Considering the present value of charging energy and channel (dot) size, it can be concluded that the channel length, width, and SOI thickness should be scaled down to 10 nm for the achievement of the room-temperature operation with the single-electron addition energy  $E_a \sim 1$  V, which is sufficient for practical applications.

In summary, we have implemented a degenerately doped SOI MOSFET with a mesoscopic-dimension channel region. Detailed analysis has been carried out to elucidate the degree of doping concentration, and the electrical and thermal characterization of degenerately doped QDs. The experimental results show that single-electron tunneling is based on band-to-band transport through a Si QD with a degenerately doped valence band, and that SETs can be made by degenerate doping in SOI MOSFETs. Coulomb oscillations were observed even at 220 K by a geometrically well-defined island and two  $p^+-n^+$  tunnel junctions in the self-aligned structure by the conventional process technology.

This work has been supported by the BK21 Program and "Development of Nanoelectronic Devices and Circuit Technology" from Korean Ministry of Commerce, Industry, and Energy.

- <sup>1</sup>D. V. Averin and K. K. Likharev, *J. Low Temp. Phys.* **62**, 345 (1986).
- <sup>2</sup>K. K. Likharev, *IEEE Trans. Magn.* **23**, 1142 (1987).
- <sup>3</sup>T. A. Fulton and G. J. Dolan, *Phys. Rev. Lett.* **59**, 109 (1987).
- <sup>4</sup>J. H. F. Scott-Thomas, S. B. Field, M. A. Kastner, H. I. Smith, and D. A. Antoniadis, *Phys. Rev. Lett.* **62**, 583 (1989).
- <sup>5</sup>R. A. Smith and H. Ahmed, *J. Appl. Phys.* **81**, 2699 (1997).
- <sup>6</sup>M. Sanquer, M. Specht, L. Ghenim, S. Deleonibus, and G. Guegan, *Phys. Rev. B* **61**, 7249 (2000).
- <sup>7</sup>N. Takahashi, H. Ishikuro, and T. Hiramoto, *Appl. Phys. Lett.* **76**, 209 (2000).
- <sup>8</sup>D. H. Kim, S.-K. Sung, J. S. Sim, K. R. Kim, J. D. Lee, B.-G. Park, B. H. Choi, S. W. Hwang, and D. Ahn, *Appl. Phys. Lett.* **79**, 3812 (2001).
- <sup>9</sup>K. Uchida, J. Koga, R. Ohba, S. Takagi, and A. Toriumi, *J. Appl. Phys.* **90**, 3551 (2001).
- <sup>10</sup>Y. Ono and Y. Takahashi, *Appl. Phys. Lett.* **82**, 1221 (2003).
- <sup>11</sup>W. H. Richardson, *Appl. Phys. Lett.* **71**, 1113 (1997).
- <sup>12</sup>J. Park and P. L. McEuen, *Appl. Phys. Lett.* **79**, 1363 (2001).
- <sup>13</sup>J. Kong, Jien Cao, H. Dai, and E. Anderson, *Appl. Phys. Lett.* **80**, 73 (2002).
- <sup>14</sup>R. S. Burton and G. M. Grivina, U.S. Patent No. 5,667,632 (16 September 1997).
- <sup>15</sup>S.-K. Sung, Y.-J. Choi, J. D. Lee, and B.-G. Park, *J. Korean Phys. Soc.* **35**, 693 (1999).
- <sup>16</sup>K. R. Kim, D. H. Kim, J. D. Lee, and B.-G. Park, *Abstracts of Si Nanoelectronics Workshop*, Kyoto, Japan, June 2001, p. 42.
- <sup>17</sup>P. A. Lee and A. D. Stone, *Phys. Rev. Lett.* **55**, 1622 (1985).
- <sup>18</sup>A. Hartstein, *Appl. Phys. Lett.* **59**, 2028 (1991).
- <sup>19</sup>*Single Charge Tunneling*, edited by H. Grabert and M. H. Devoret (Plenum, New York, 1992).
- <sup>20</sup>M. G. Peters, S. G. den Hartog, J. I. Dijkhuis, O. J. A. Buyk, and L. W. Molenkamp, *J. Appl. Phys.* **84**, 5052 (1998).